Fluid elasticity and the transition to chaos in thermal convection

Roger E. Khayat
National Research Council of Canada, Industrial Materials Institute, 75, de Mortagne Boulevard, Boucherville, Quebec, Canada J4B 6Y4

(Received 9 May 1994; revised manuscript received 9 September 1994)

The influence of fluid elasticity on the onset of aperiodic or chaotic motion of an upper-convected Maxwellian fluid is examined in the context of the Rayleigh-Bénard thermal convection problem. A truncated Fourier representation of the flow and temperature fields leads to a four-dimensional dynamical system that constitutes a generalization of the classical Lorenz system for Newtonian fluids. It is found that, to the order of the present truncation and above a critical value of the Deborah number De^c, steady convection cannot set in, with the fluid becoming overstable instead. For $De < De^c$, and even close to the Newtonian limit, the presence of fluid elasticity appears to alter significantly the circumstances leading to the onset of chaotic motion. Depending on the value of the Prandtl number, chaos is found to set in through the quasiperiodic route or period doubling. In general, fluid elasticity tends to destabilize the convective cell structure, precipitating the onset of chaos, at a Rayleigh number that may be well below that corresponding to Newtonian fluids.

PACS number(s): 47.50.+d, 05.45.+b, 64.10.+h

I. INTRODUCTION

The simplicity of the Lorenz equations, and the rich sequence of flow phenomena exhibited by their solution, have been the major contributing factors to their widespread use as a model for examining the onset of chaotic motion. Despite the severe truncation in the formulation of these equations, some of the basic qualitative elements at the onset of the steady thermal convection and during its subsequent destabilization have been recovered through the model. Yet, quite a few important experimental phenomena observed in the case of low molecular weight fluids (including supposedly "Newtonian" fluids) cannot be recovered by such an apparently simple model. Whether such a discrepancy between theory and experiment is solely due to the severity of truncation, or the inadequacy of the Navier-Stokes-Fourier equations altogether to describe the flow in the transition regime, remains an open question.

Newton's law of viscosity and Fourier's law of heat are based on linear irreversible thermodynamics [1]. They do not account for any dependence of the transport coefficients on shear rate or temperature gradient. Such a limitation is not so severe as long as one is interested in flows close to equilibrium. For flows far from equilibrium, such as in the transition regime, nonlinear effects become significant. These nonlinearities manifest themselves in the form of shear thinning, for shear rate dependent viscosity, or in the form of normal stresses leading to the so-called Weissenberg rod-climbing effect. Such nonlinear effects must then somehow be accounted for in the constitutive model if an accurate description in the transition regime is to be achieved. In this paper, we focus our attention on the influence of fluid elasticity or normal stresses on the stability of the two-dimensional cellular structure and onset of chaos during thermal convection.

If normal stresses manifest themselves in fluids with significant relaxation time, then viscoelastic behavior should not be regarded as exclusive to polymeric liquids. Rarefied gases and supercooled monatomic liquids are just examples of fluids that exhibit non-negligible elastic behavior under normal conditions of flow [2–4]. The kinetic theory foundation of constitutive models for monatomic dilute (dense) Lennard-Jones fluids, based on the (generalized) Boltzmann equation, clearly shows the viscoelastic character of such fluids [5–7]. The major distinction in constitutive behavior between monatomic fluids and polyatomic liquids appears to lie in the form of the transport coefficients of viscosity and normal stress [8]. More generally, *all* fluids possess some degree of elasticity. Fluid elasticity was estimated by Derjaguin *et al.* [9] through the resonance technique for low-viscosity liquids such as water, cyclohexane, hexadecane, and dibutylphalate. These liquids were found to possess a shear elasticity of about 10^6 dyn/cm^2 at a frequency of shear oscillations of about 73.5 kHz, that is, at a frequency 6–7 orders of magnitude lower than what is usually believed. Earlier prediction and measurements by Joseph and coworkers [10–12] of the shear-wave speeds and elastic moduli of several supposedly "Newtonian" liquids also indicate that such liquids do possess a non-negligible degree of elasticity. In addition to this intrinsic elastic property of fluids under normal conditions of flow, it is well established that fluid elasticity or normal stresses tend to become rather pronounced under conditions of high deformation rate, heat, and/or diffusion fluxes.

Khayat and Eu [13] examined in detail the influence of normal stresses and thermoviscous dissipative coupling on the Taylor-Couette flow of Lennard-Jones fluids. The viscoelastic behavior of such fluids is dictated by the so-called generalized hydrodynamic equations for stress and heat flux. These equations are derived on the basis of the modified moment method for the solution of the (general-

ized) Boltzmann equation for dilute (dense) monatomic fluids [7], and lead to flow and temperature fields similar to those obtained by the Navier-Stokes-Fourier equations in the limit of small thermodynamic gradients. Numerical calculations using these apparently *laminar* equations show that, by properly accounting for normal stresses in the constitutive equations, one can predict the sudden drop in drag coefficient as the Reynolds number reaches a critical value [13(c)]. The flow behavior was also found to approach that of an ideal fluid as the Reynolds number was further increased, while normal stresses become increasingly dominant. These findings seem to suggest that such elastic or normal stress effects *for any fluid* are bound to become significant under extreme flow conditions, particularly in the transition and turbulent regimes. What is then the influence of fluid "elasticity" on the spatiotemporal structure of the flow as it evolves towards the turbulent regime?

To examine this question, Khayat [14] developed a four-dimensional dynamical system for the thermal convection of strongly elastic flows of the Oldroyd-B type. Such a system constitutes a generalization of the Lorenz equations [15] to include viscoelastic fluids. The critical Rayleigh number at the onset of the convective cellular structure was found to be the same as for Newtonian fluids. This is a direct consequence of the fact that the nonlinear terms (at least to the degree of truncation adopted) are the same as those in the Lorenz equations; no convective or upper-convective nonlinear terms survive in the constitutive equations. The conductive state thus loses its stability to the two steady convective branches C_1 and C_2, say, through a supercritical bifurcation similarly to Newtonian fluids. The stability of the conductive state near the onset of the convective branches was later examined [16] by applying the center manifold theorem [17]. The two convective branches lose their stability in turn through a Hopf bifurcation as the Rayleigh number exceeds a value which, this time, depends strongly on fluid elasticity and retardation. It was also observed that fluid elasticity tends to precipitate the onset of chaotic motion, while fluid retardation tends to delay it. Above a critical value for the Deborah number, which for an upper-convected Maxwellian (UCM) fluid is given by $\mathrm{De}^c=(1+\mathrm{Pr}^{-1})(\pi^2+q^2)^{-1}$, Pr being and Prandtl number and q the wave number, the flow behavior departs significantly from that of a Newtonian fluid. All three fixed branches remain unstable in the supercritical range for any value of the Rayleigh number. Thus, for $\mathrm{De}>\mathrm{De}^c$, no steady convection can set in, and the cellular structure is always periodic in time (overstable), with the corresponding Fourier spectrum showing sharp peaks at the fundamental frequency and its harmonics that tend to increase in number as De increases.

In this paper, we focus our attention on the influence of fluid elasticity on the destabilization of steady convection and onset of chaotic motion for weakly elastic fluids ($\mathrm{De}<\mathrm{De}^c$). More particularly, we examine the role elasticity may play in the birth and stability of the Hopf bifurcation at the postcritical Rayleigh number $\mathrm{Ra}_h>\mathrm{Ra}_c$, just before chaos sets in. To this end, a multiple-scales perturbation analysis is carried out around Ra_h in order to determine the stability of the periodic orbit. It is a well established fact that in the case of the Lorenz equations [18], the solution is not attracted toward a periodic limit cycle. Instead, it undergoes a homoclinic bifurcation and then becomes chaotic as Ra is further increased. Some special attention is also paid to the influence of the Prandtl number. Rather than adopting a sophisticated viscoelastic constitutive model, be it kinetic theory based [8,19] or phenomenological [20], we will assume that the fluid under investigation obeys the less realistic Maxwell equation. The choice of a suitable constitutive model is not crucial at this stage, since our initial objective is to bring out the fundamental role elasticity can play in the transition regime.

II. PROBLEM FORMULATION

The derivation of the four-dimensional dynamical system for a Maxwellian fluid is discussed in this section. Since a detailed derivation as well as the coherence of the model have been given elsewhere for an Oldroyd-B fluid [14], only the main points are discussed here. Note that Maxwell's equation is obtained from the Oldroyd-B equation by setting fluid retardation to zero. First, some of the basic assumptions involved in the general governing (conservation and constitutive) equations and boundary conditions for the thermal convection of a viscoelastic fluid are briefly reviewed. A truncated Fourier representation of the general solution is then introduced, leading to the four-dimensional system, which constitutes a generalization of Lorenz model to include viscoelastic fluids.

A. Governing equations and boundary conditions

Consider a viscoelastic fluid placed horizontally between two flat plates separated by a distance D. The x axis is taken along the plates lying halfway in between, the z axis is in the direction perpendicular to the plates. Let T_0 and $T_0+\delta T$ be the temperatures of the upper and lower plates, respectively, with δT being the temperature difference. T_0 is taken as the reference temperature. In the present work, the substances of main interest are assumed to obey the following equation of state:

$$\rho^*=\rho_0[1-\alpha_T(T^*-T_0)] , \tag{1}$$

where ρ^* and ρ_0 are the densities at T^* and T_0, respectively, and α_T is the coefficient of volumetric expansion. If the Boussinesq approximation, which states that the effect of compressibility is negligible everywhere in the conservation equations except in the buoyancy term, is assumed to hold, then the equations for conservation of mass, momentum, and energy, for the departure from the pure conductive state, read, respectively,

$$\nabla\cdot\mathbf{u}=0 , \tag{2}$$

$$\mathrm{Pr}^{-1}\left[\frac{\partial\mathbf{u}}{\partial t}+\mathbf{u}\cdot\nabla\mathbf{u}\right]=-\nabla p-\nabla\cdot\tau+\theta\mathbf{k} , \tag{3}$$

$$\frac{\partial\theta}{\partial t}+\mathbf{u}\cdot\nabla\theta=\nabla^2\theta+\mathrm{Ra}\mathbf{u}\cdot\mathbf{k}-\mathrm{Ra}\,\mathrm{Pr}\,\mathrm{Ec}\tau:\nabla\mathbf{u} , \tag{4}$$

where ∇ is the two-dimensional gradient operator, $\mathbf{u}(u,w)$ is the velocity vector, p is the hydrostatic pressure, τ is the deviatoric stress tensor. $\theta=(T^*-T_s^*)/\delta T$ is the departure from the steady-state temperature T_s^*, and $\mathbf{k}$ is the unit vector along the z direction. Equations (2)–(4) must be supplemented with a constitutive equation for τ. The constitutive equation for stress is taken to correspond to an upper-convected Maxwellian fluid [20]:

$$\frac{\partial\tau}{\partial t}+\mathbf{u}\cdot\nabla\tau-\nabla\mathbf{u}^t\cdot\tau-\tau\cdot\nabla\mathbf{u}=-\mathrm{De}^{-1}(\tau+\gamma)\ , \tag{5}$$

where $\gamma=\nabla\mathbf{u}+\nabla\mathbf{u}^t$ is the rate-of-strain tensor. The following dimensionless groups were introduced, namely the Rayleigh number, Prandtl number, Eckert number, and Deborah number:

$$\mathrm{Ra}=\frac{\delta T g\alpha_T D^4}{\nu_0\kappa}\ ,\quad \mathrm{Pr}=\frac{\nu_0}{\kappa}\ ,\quad \mathrm{Ec}=\frac{\kappa^2}{C_v\delta T D^2}\ ,\quad \mathrm{De}=\frac{\lambda\kappa}{D^2}\ , \tag{6}$$

with ν_0 being the zero-shear-rate kinematic viscosity, λ the relaxation time, $\kappa=K/(\rho_0 C_v)$ the thermometric conductivity, K the thermal conductivity, C_v the specific heat at constant volume, and g the acceleration due to gravity. Thus, De is a measure of fluid elasticity. The characteristic time, length, velocity, and pressure were taken to be D^2/κ, D, κ/D, and $\rho\nu_0\kappa/D^2$, respectively. Appropriate boundary conditions must now be examined.

Since the fluid is confined between the planes $z=-\frac{1}{2}$ and $z=+\frac{1}{2}$, regardless of the nature of the two surfaces, one must have

$$\theta(x,z=-\tfrac{1}{2},t)=\theta(x,z=+\tfrac{1}{2},t)=0\ , \tag{7}$$

$$w(x,z=-\tfrac{1}{2},t)=w(x,z=+\tfrac{1}{2},t)=0\ , \tag{8}$$

since the temperature is fixed at the bounding planes, and the normal velocity component is zero. There are two remaining boundary condition which, however, depend on the nature of the two bounding surfaces. It will be assumed that the two planes are free surfaces on which the tangential stress components are equal to zero. Thus,

$$\tau_{xz}(x,z=\pm\tfrac{1}{2},t)=0\ . \tag{9}$$

Since the problem is two dimensional, one may conveniently introduce a stream function $\psi(x,z,t)$ such that

$$u=-\psi_{,z}\ ,\quad w=\psi_{,x}\ , \tag{10}$$

where a subscript comma denotes partial differentiation. In this case, one may take the curl of Eq. (3), and eliminate the pressure to obtain

$$\mathrm{Pr}^{-1}(\Delta\psi_{,t}-\psi_{,z}\Delta\psi_{,x}+\psi_{,x}\Delta\psi_{,z})=\theta_{,x}-(\tau_{zz}-\tau_{xx})_{,xz}-\tau_{xz,xx}+\tau_{xz,zz}\ , \tag{11}$$

where $\Delta=\partial^2/\partial x^2+\partial^2/\partial z^2$ is the Laplacian operator. Since $\mathrm{Ra\,Pr\,Ec}=g\alpha_T D^2/C_v$, and for most fluids of interest α_T is of the order 10^{-2} to 10^{-4}, the work term in the heat transport equation (4) may be neglected, thus leading to

$$\theta_{,t}+\psi_{,x}\theta_{,z}-\psi_{,z}\theta_{,x}=\mathrm{Ra}\psi_{,x}+\Delta\theta\ . \tag{12}$$

From Eq. (5) the stress tensor components are governed by

$$\tau_{xx,t}+\psi_{,x}\tau_{xx,z}-\psi_{,z}\tau_{xx,x}+2\psi_{,xz}\tau_{xx}+2\psi_{,zz}\tau_{xz}=-\mathrm{De}^{-1}(\tau_{xx}-2\psi_{,xz})\ , \tag{13}$$

$$\tau_{yy,t}+\psi_{,x}\tau_{yy,z}-\psi_{,z}\tau_{yy,x}=-\mathrm{De}^{-1}\tau_{yy}\ , \tag{14}$$

$$\tau_{zz,t}+\psi_{,x}\tau_{zz,z}-\psi_{,z}\tau_{zz,x}-2\psi_{,xx}\tau_{xz}-2\psi_{,zx}\tau_{zz}=-\mathrm{De}^{-1}(\tau_{zz}+2\psi_{,xz})\ , \tag{15}$$

$$\tau_{xz,t}+\psi_{,x}\tau_{xz,z}-\psi_{,z}\tau_{xz,x}-\psi_{,xx}\tau_{xx}+\psi_{,zz}\tau_{zz}=-\mathrm{De}^{-1}(\tau_{xz}+\psi_{,xx}-\psi_{,zz})\ . \tag{16}$$

It is useful to note that the τ_{yy} component of the stress tensor, governed by Eq. (14), is decoupled from the rest of the equations and boundary conditions. Thus, the lack of any boundary conditions forces τ_{yy} to be independent of x and z, except through its coupling with ψ. Thus, the evolution of τ_{yy} can be determined separately from the rest of the flow and temperature fields, and therefore will not be considered any further.

B. The four-dimensional dynamical system

The solution to Eqs. (11)–(16), subject to boundary conditions (7)–(9), may be represented by an infinite Fourier series in x and z, with the series coefficients depending on time alone. One then ends up with an infinite set of ordinary differential equations. In practice, however, one seeks a way to truncate the Fourier series to obtain a finite-dimensional system of ordinary differential equations. The truncation cannot be arbitrary since the truncated form of the solution must still satisfy the imposed boundary conditions. In the present work, an additional restriction imposes itself naturally on the truncated solution: the resulting dynamical system must reduce to the Lorenz equations in the limit $\mathrm{De}\to 0$. In a manner similar to the case of a Newtonian fluid [15,21], only one term in the Fourier representation for the stream function is kept:

$$\psi(x,z,t)=\psi_1(t)\sin(qx)\cos(\pi z)\ , \tag{17}$$

which satisfies boundary conditions (8). Here $2\pi/q$ is the (imposed) period in the x direction. Since the stress tensor is coupled to the velocity field through Eqs. (13)–(16), the same periodicity in x may be imposed, thus

$$\tau_{xx}(x,z,t)=\xi(t)\cos(qx)\sin(\pi z)\ , \tag{18}$$

$$\tau_{zz}(x,z,t)=\zeta(t)\cos(qx)\sin(\pi z)\ , \tag{19}$$

$$\tau_{xz}(x,z,t)=\sigma(t)\sin(qx)\cos(\pi z)\ . \tag{20}$$

Note that these expressions, together with (17), satisfy boundary conditions (9). A similar argument holds for the temperature. However, as in the case of Newtonian fluid, more than one term is needed in the temperature expression if some part of the nonlinearities in Eqs. (11)–(16) is to be retained. Here, again, following Lorenz

[15], one may set

$$\theta(x,z,t)=\theta_1(t)\cos(qx)\cos(\pi z)+\theta_2(t)\sin(2\pi z) . \quad (21)$$

Projecting Eqs. (11)–(16) onto modes (17)–(21), one obtains the following four-dimensional system [14]:

$$\dot{X}=\mathrm{Pr}(Y-P) , \quad (22)$$

$$\dot{Y}=-XZ+rX-Y , \quad (23)$$

$$\dot{Z}=XY-bZ , \quad (24)$$

$$\dot{P}=\delta(X-P) , \quad (25)$$

where a dot denotes the $\tau d/dt$ operator,

$$\delta=\frac{\tau}{\mathrm{De}} , \quad \tau=\frac{1}{\pi^2+q^2} , \quad a=\frac{q}{\pi} ,$$

$$X=\frac{\pi q\tau}{\sqrt{2}}\psi_1 , \quad Y=\frac{\pi q^2\tau^3}{\sqrt{2}}\theta_1 , \quad Z=\frac{\pi q^2\tau^3}{\sqrt{2}}\theta_2 ,$$

$$P=\frac{q\tau}{\pi\sqrt{2}}[a(\zeta-\xi)+(a^2-1)\sigma] .$$

As in the case of the Lorenz equations, it is convenient to introduce the following parameters:

$$r=\frac{q^2}{(\pi^2+q^2)^3}\mathrm{Ra} , \quad b=\frac{4}{a^2+1} . \quad (26)$$

In the limit $\mathrm{De}\to 0$, that is, in the case of a Newtonian fluid, Eqs. (22)–(25) reduce to the Lorenz equations [15]

$$\dot{X}=\mathrm{Pr}(Y-X) , \quad \dot{Y}=-XZ+rX-Y , \quad \dot{Z}=XY-bZ . \quad (27)$$

It is important to observe that the nonlinear terms in the viscoelastic Eqs. (22)–(25) are exactly the same as those in the Newtonian Eqs. (27); they stem only from the convective terms in the energy equation. Indeed, there are no nonlinearities retained from the convective or upper convective terms in the stress equations, at least to the order of truncation taken in the present work.

III. THE STEADY-STATE SOLUTIONS AND THEIR STABILITY

Before attempting the numerical solution of Eqs. (22) and (25), it would be useful to examine the local stability of the equilibrium points in order to unravel some of the fundamental difference between Newtonian and viscoelastic fluids. Although the truncated constitutive equation (25) is equivalent to the linear Maxwell equation, it is expected to alter the spatiotemporal structure and stability picture. For a very small value of De, one expects the behavior of the flow in phase space to be similar in both the Newtonian and viscoelastic regimes, at least around the purely conductive state. As De increases, the stability picture changes for viscoelastic fluids, giving rise to a stable periodic solution.

A. Steady-state solutions

In the absence of additional nonlinearity from the constitutive equations, the steady-state solutions for velocity and temperature are the same as those of the Lorenz equations. There is one trivial solution, that is, the origin in phase space:

$$X_S=Y_S=Z_S=P_S=0 , \quad (28)$$

which corresponds to pure heat conduction. As r exceeds unity, two additional fixed branches C_1 and C_2 emerge, corresponding to the onset of (two-dimensional) convective rolls in opposite directions:

$$X_S=Y_S=\pm[b(r-1)]^{1/2} , \quad Z_S=r-1 ,$$
$$P_S=\pm[b(r-1)]^{1/2} . \quad (29)$$

Thus, the critical value of the Rayleigh number at the onset of steady convection does not depend on De. In other words, at least on the basis of the present model, the critical Rayleigh number and wave number at the onset of the cellular structure for a viscoelastic fluid are the same as those for a Newtonian fluid. This important conclusion could have been anticipated earlier by noting that, under steady-state conditions, Eqs. (22)–(25) reduce to the steady Lorenz equations. This result is in agreement with the experiments of Liang and Acrivos [22]. The expression for the critical value of the Rayleigh number is then given by

$$\mathrm{Ra}_c=\frac{(\pi^2+q^2)^3}{q^2} , \quad (30)$$

so that the wave number for the minimum value of Ra_c is equal to $q_c=\pi/\sqrt{2}$. In the calculations below, the value of q is taken equal to q_c. The stability of the conductive state was examined previously in some detail [14,16]. In the present work, we focus our attention on the existence and stability of the Hopf bifurcation when C_1 and C_2 lose their stability before chaotic motion eventually sets in. For completeness, the general stability picture is summarized first.

B. Stability of the steady-state solutions

The results based on linear stability analysis of Eqs. (22)–(25) are summarized in Fig. 1. Linear stability analysis around the origin leads to an obvious characteristic value: $\lambda=-b$, while the remaining three roots are governed by

$$\lambda^3+(\delta+1)\lambda^2+(\mathrm{Pr}\delta+\delta-r\,\mathrm{Pr})\lambda+\mathrm{Pr}\delta(1-r)=0 . \quad (31)$$

In the limit of a Newtonian fluid, that is, as $\mathrm{De}\to 0$, Eq. (31) reduces to

$$\lambda^2+(\mathrm{Pr}+1)\lambda+\mathrm{Pr}(1-r)=0 . \quad (32)$$

The roots of this equation are always real since $r>0$, and one of them becomes positive as r exceeds 1. That is when the origin loses its stability to the two other steady-state solutions coinciding with the onset of the (two-dimensional) convection rolls. In the case of a viscoelastic fluid and at small De value, Eq. (31) leads to a similar exchange of stability which takes place at $r=1$ when a supercritical bifurcation emerges as shown in Fig. 1(a). The conductive state, which is stable for $r<1$, loses

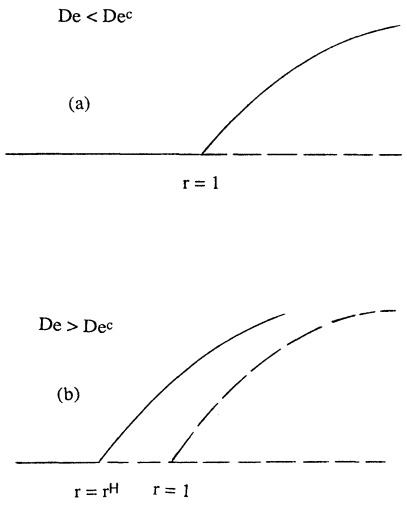

FIG. 1. Bifurcation diagram around the conductive state for (a) weakly elastic flow ($De < De^c$) and (b) strongly elastic flow ($De > De^c$). Stable and unstable solution branches are indicated by solid and dashed lines, respectively. Note the birth of a precritical Hopf bifurcation (at $r = r^H < 1$) when $De > De^c$. In this case, no steady convection sets in.

its stability to the two convective branches as r exceeds unity. The emergence of the branches C_1 and C_2 corresponds to the onset of steady convection. Thus, for $r > 1$, the solution evolves to either one of the branches depending on the initial conditions. As r increases and reaches a critical value $r_H(\mathrm{De},\mathrm{Pr}) > 1$, the two convective states lose their stability through a Hopf bifurcation. In this case, the solution tends to "hover" from around one branch to the other passing through the origin, and eventually remains locked (in phase space) on what is now well established as the strange attractor. This situation persists as long as De remains smaller than a critical value, namely, $De^c = \tau(\mathrm{Pr}+1)/\mathrm{Pr}$.

As De exceeds De^c, stability analysis around $r = 1$ shows that both the origin and the two convective branches are unstable [16] as shown in Fig. 1(b). In the range $r < 1$, a Hopf bifurcation emerges at $r = r^H(\mathrm{De},\mathrm{Pr})$, corresponding to the onset of overstability or periodic solution. The origin was found to be stable for $r < r^H$ and unstable for $r > r^H$. Thus, the solution would evolve towards the conductive state in the former case, while it ends up on a periodic orbit in the latter. The stability of the periodic orbit was later confirmed by applying the center manifold theorem around $r = r^H < 1$ [23]. Note that although the birth on the Hopf bifurcation occurs at a precritical r value ($r^H < 1$), a limit cycle usually exists for the solution at $r > 1$. Thus, when $De > De^c$, the branches C_1 and C_2 are always unstable, and the solution settles into periodic orbit even after r has exceeded unity. Thus, for strongly elastic fluids ($De > De^c$), steady convection cannot set in when the Rayleigh number exceeds Ra_c. This is of course in sharp contrast to the case of weakly elastic fluids ($De < De^c$) where steady convection always sets in for $r > 1$, with C_1 and C_2 losing their stability through a Hopf bifurcation at $r = r_H$. One is then confronted with the question regarding the nature of the solution for $r > r_H$; more particularly, what role does fluid elasticity play after the two convective branches lose their stability? It is precisely to this question that we now turn.

IV. EXISTENCE AND STABILITY OF A HOPF BIFURCATION FOR WEAKLY ELASTIC FLUIDS

We now examine the conditions for the emergence and stability of a postcritical Hopf bifurcation (at $r = r_H > 1$) when $De < De^c$. To this end, multiple-scales perturbation analysis is carried out for an r value slightly above r_H. Linear stability analysis around the fixed branches (29) leads to the following characteristic equation for the eigenvalues:

$$\Delta(\lambda)=\lambda^4+(b+1+\delta)\lambda^3+[br-\mathrm{Pr}+\delta(\mathrm{Pr}+b+1)]\lambda^2 +[b\,\mathrm{Pr}(r-2)+\delta b(\mathrm{Pr}+r)]\lambda+2\delta\,\mathrm{Pr}(r-1)=0\ . \tag{33}$$

In the limit $De \to 0$, one recovers the characteristic equation for the Lorenz system:

$$\lambda^3+(\mathrm{Pr}+b+1)\lambda^2+b(\mathrm{Pr}+r)\lambda+2\,\mathrm{Pr}b(r-1)=0\ . \tag{34}$$

Thus, for a Newtonian fluid, the two nontrivial fixed points C_1 and C_2 are sinks for $r \in (1, \mathrm{Pr}(\mathrm{Pr}+b+3)(\mathrm{Pr}-b-1)^{-1})$. At $r = 1$, a pitchfork bifurcation occurs, while the origin is a saddle point with a one-dimensional unstable manifold. A Hopf bifurcation occurs when (34) possesses a pair of purely imaginary roots. In this case, the value r_H^{Newt} of r when this occurs and the initial (dimensionless) frequency ω_{Newt} are given by

$$r_H^{\mathrm{Newt}}=\mathrm{Pr}\frac{\mathrm{Pr}+b+1}{\mathrm{Pr}-b-1}\ ,\quad \omega_{\mathrm{Newt}}^2=2b\,\mathrm{Pr}\frac{\mathrm{Pr}+1}{\mathrm{Pr}-b+1}\ . \tag{35}$$

For $r > r_H^{\mathrm{Newt}}$, C_1 and C_2 are saddles with two-dimensional unstable manifolds. Thus, for $r > r_H^{\mathrm{Newt}}$ all three fixed points are unstable, but an attracting region in phase space still exists which, for $\mathrm{Pr} = 10$, $b = \frac{8}{3}$, and $r = 28$, is known as the Lorentz attractor. At low De value, one expects a similar (Hopf) bifurcation to emerge in the case of viscoelastic fluids. In the case of the Lorenz system, however, the periodic orbit coinciding with the Hopf bifurcation is found numerically to be unstable. The question we are about to examine is whether fluid elasticity has any stabilizing effect in forcing the phase trajectory to become locked onto a limit cycle as a result of the Hopf bifurcation. But let us first look at the general conditions for existence of a postcritical Hopf bifurcation.

A. Existence of a postcritical Hopf bifurcation

The existence of a postcritical Hopf bifurcation is examined only when $De < De^c$, since otherwise steady convection does not exist. In order to find at what value r_H of r this occurs, we set $\lambda = i\omega$ in Eq. (33) and equate real

and imaginary parts to zero, to obtain the following equation for r_H:

$$2\delta\,\mathrm{Pr}(r_H-1)(b+\delta+1)^2+b[(\mathrm{Pr}+\delta)r_H+\mathrm{Pr}(\delta-2)]^2 -b[(\mathrm{Pr}+\delta)r_H+\mathrm{Pr}(\delta-2)][br_H-\mathrm{Pr}+\delta(b+\mathrm{Pr}+1)] \times(b+\delta+1)=0\ , \quad (36a)$$

with the expression for ω given by

$$\omega^2=b\frac{(\mathrm{Pr}+\delta)r_H+\mathrm{Pr}(\delta-2)}{b+\delta+1}\ , \quad \mathrm{De}<\mathrm{De}^c=\frac{\tau(\mathrm{Pr}+1)}{\mathrm{Pr}}\ . \quad (36b)$$

The inequality in (36b) insures that a postcritical Hopf bifurcation does not exist for strongly elastic flows ($\mathrm{De}>\mathrm{De}^c$). In the limit $\mathrm{De}\to 0$, one recovers the Newtonian expressions (35). Equation (36a) is a second-order equation in r_H. Note that $r_H(\mathrm{De}=\mathrm{De}^c)=1$. Figure 2 shows the ($r_H-\mathrm{De}$) curves for moderate values of the Prandtl number. The end of the curves coincides with ($r_H=1$, $\mathrm{De}=\mathrm{De}^c$). For $\mathrm{Pr}=4.5$ and 10, r_H decreases monotonically with De. Thus, for such moderately small values of the Prandtl number, fluid elasticity tends to precipitate the destabilization of steady convection. For $\mathrm{Pr}=25$ and 35, there is a maximum that appears at a relatively small De value. In this case, a low level of fluid elasticity tends to stabilize steady convection by raising the value of r_H. In general, a leveling of the curve, however, begins to occur at relatively small De value. Thus, a relatively small amount of fluid elasticity tends to decrease dramatically the value of r_H, to a value close to unity. We will examine the implications of the results in Fig. 2 later when numerical solutions are presented.

B. Stability of the Hopf bifurcation

We have just established that a Hopf bifurcation comes into existence at $r=r_H$. Thus, from linear stability analysis, we are led to believe that at $r=r_H$, a limit cycle of frequency ω will be formed when the numerical solution is performed. Such a limit cycle is, however, not always found. This is indeed the case of the solution of the Lorenz equations which does not display a periodic orbit as predicted by expressions (35). Whether this situation is altered under the influence of fluid elasticity can only be established by examining the influence of the nonlinear terms in the system (22)–(25). We are particularly interested in the flow as r is increased slightly above r_H. We now carry out a multiple-scales perturbation analysis similar to that of Newell and Whitehead [24] and set $r=r_H(1+\varepsilon^2)$, where ε is a small ordering parameter.

Let us focus the analysis on the perturbation from the fixed branch C_1. If we denote the departure from C_1 by [see Eqs. (29)]

$$\mathbf{V}\equiv(U,V,W,Q)^t=(X,Y,Z,P)^t-(X_S,Y_S,Z_S,P_S)^t\ , \quad (37)$$

then upon substituting (37) into (22)–(25) and keeping terms to $O(\varepsilon^2)$, we have

$$L\begin{bmatrix}U\\V\\W\\Q\end{bmatrix}=\begin{bmatrix}0\\-UW\\UV\\0\end{bmatrix}-\varepsilon^2\frac{br_H}{2X_H}\begin{bmatrix}0&0&0&0\\0&0&1&0\\-1&-1&0&0\\0&0&0&0\end{bmatrix}\begin{bmatrix}U\\V\\W\\Q\end{bmatrix}+O(\varepsilon^3)\ , \quad (38)$$

where we have introduced

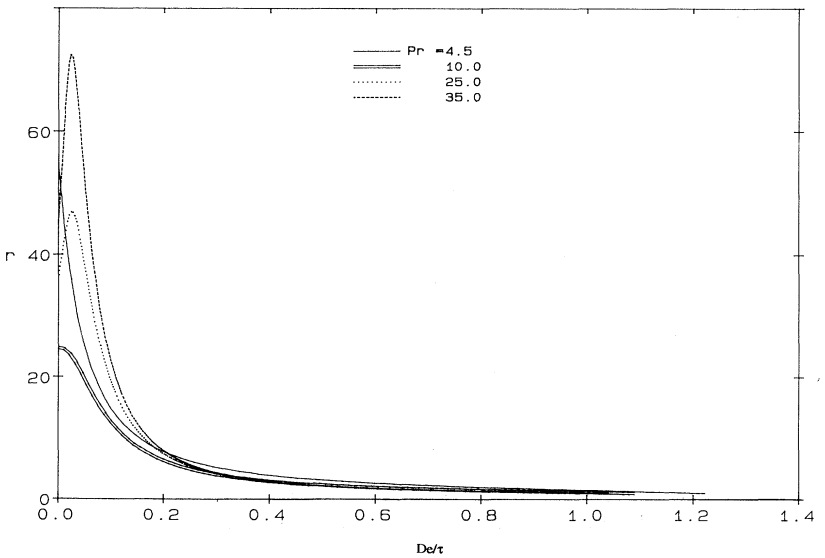

FIG. 2. Onset of postcritical Hopf bifurcation at $r=r_H$. The ($r_H-\mathrm{De}$) curves are shown as a function of the Prandtl number.

$$L \equiv \begin{bmatrix} \frac{d}{dt} & -\mathrm{Pr} & 0 & \mathrm{Pr} \\ -1 & \frac{d}{dt}+1 & X_H & 0 \\ -X_H & -X_H & \frac{d}{dt}+b & 0 \\ -\delta & 0 & 0 & \frac{d}{dt}+\delta \end{bmatrix},$$

$$X_H = +[b(r_H-1)]^{1/2} .$$

We now introduce another time scale $T=\varepsilon^2 t$ of $O(\varepsilon^2)$, and write

$$\frac{d}{dt} \rightarrow \frac{\partial}{\partial t}+\varepsilon^2\frac{\partial}{\partial T}+O(\varepsilon^3) , \quad \mathbf{V}=\sum_{n=1}\varepsilon^n \mathbf{V}_{n-1} . \tag{39}$$

Thus, to $O(\varepsilon)$, we have

$$L\mathbf{V}_0=\mathbf{0} , \tag{40}$$

where $\mathbf{V}_0$ may be expressed in terms of the eigenvectors (and their complex conjugates) of the Jacobian matrix arising from the linearization of (22)–(25) and C_1:

$$\mathbf{V}_0 = A(T)\begin{bmatrix} U_H \\ V_H \\ W_H \\ Q_H \end{bmatrix} e^{i\omega t} + A^*(T)\begin{bmatrix} U_H^* \\ V_H^* \\ W_H^* \\ Q_H^* \end{bmatrix} e^{-i\omega t} ,$$

where

$$\begin{bmatrix} U_H \\ V_H \\ W_H \\ Q_H \end{bmatrix} = \begin{bmatrix} 1 \\ \mathrm{Pr}Q_H+i\omega \\ \dfrac{X_H(V_H+1)}{b+i\omega} \\ \dfrac{\delta}{\delta+i\omega} \end{bmatrix} \tag{41}$$

and $A(T)$ is a slowly varying function of T. Note that $\mathbf{V}_0$ is the form of the limit cycle to $O(\varepsilon)$, and in order for the limit cycle to be detected by the numerical solution, the real part of $A(T)$ must not grow indefinitely with respect to T. The conditions for growth or decay can be determined through an appropriately derived equation for A by examining higher-order terms.

To $O(\varepsilon^2)$, Eq. (38) leads to the following equation for $\mathbf{V}_1$ [after substitution of (41)]:

$$L\mathbf{V}_1 = |A|^2\begin{bmatrix} 0 \\ -W_H-W_H^* \\ V_H+V_H^* \\ 0 \end{bmatrix} + A^2\begin{bmatrix} 0 \\ -W_H \\ V_H \\ O \end{bmatrix} e^{2i\omega t} + A^{*2}\begin{bmatrix} 0 \\ -W_H^* \\ V_H^* \\ 0 \end{bmatrix} e^{-2i\omega t} , \tag{42}$$

which can be easily solved to give

$$\mathbf{v}_1 = |A|^2\begin{bmatrix} \alpha \\ \alpha \\ -\dfrac{W_H+W_H^*}{X_h} \\ \alpha \end{bmatrix} + A^2\begin{bmatrix} \beta \\ \chi \\ X_H^{-1}[\beta-(1+2i\omega)\chi-W_H \\ \dfrac{\delta}{\delta+i\omega} \end{bmatrix} e^{i\omega t}+\text{c.c.} , \tag{43}$$

where

$$\alpha = -\frac{\delta\,\mathrm{Pr}}{\Delta(0)}[b(W_H+W_H^*)+X_H(V_H+V_H^*)] ,$$

$$\beta = -\frac{\delta\,\mathrm{Pr}}{\Delta(2i\omega)}[(b+2i\omega)W_H+X_H V_H](\delta+2i\omega) , \quad \chi = \frac{\beta}{\mathrm{Pr}}\left[\frac{\delta\,\mathrm{Pr}}{\delta+2i\omega}+2i\omega\right] ,$$

Δ being defined by Eq. (33). Note that the solution to (41) was obtained without leading to any constraint on A. Such a constraint is obtained when the next order in ε is examined. Thus, to $O(\varepsilon^3)$, we have

$$L\mathbf{V}_2 = -\frac{dA}{dT}\begin{bmatrix} 1 \\ V_H \\ W_H \\ Q_H \end{bmatrix} e^{i\omega t}+\text{c.c.} - \frac{br_H}{2X_H}\begin{bmatrix} 0 & 0 & 0 & 0 \\ 0 & 0 & 1 & 0 \\ -1 & -1 & 0 & 0 \\ 0 & 0 & 0 & 0 \end{bmatrix}\begin{bmatrix} U_0 \\ V_0 \\ W_0 \\ Q_0 \end{bmatrix} + \begin{bmatrix} 0 \\ -W_0U_1-U_0W_1 \\ V_0U_1+U_0V_1 \\ 0 \end{bmatrix} . \tag{44}$$

Upon substitution of (41) and (43) into the right hand side of (44), one observes the emergence of secular terms as far as the determination of $\mathbf{V}_2$ is concerned. The solvability condition for Eq. (44), after extensive algebraic manipulation, leads to the following constraint equation on $A(T)$:

$$(c_1+V_Hc_2+W_Hc_3+Q_Hc_4)\frac{dA}{dT}$$
$$=\frac{br_H}{2X_H}[(1+V_H)c_3-W_Hc_2]A$$
$$+\left[c_3[(V_H+1)\alpha+\chi+\beta V_H^*]-c_2\left[W_H\alpha+\frac{\beta-(1+2i\omega)\chi-2W_H-W_H^*}{X_H}+W_H^*\beta\right]\right]|A^2|A\ , \tag{45}$$

where the following complex valued quantities were introduced:

$$c_1=\delta br_H-\omega^2(b+\delta+1)+i\omega(br_H+b\delta+\delta-\omega^2)\ ,\quad c_2=\mathrm{Pr}[b\delta-\omega^2+i\omega(b+\delta)]\ ,$$
$$c_3=-X_H\mathrm{Pr}(\delta+i\omega)\ ,\quad c_4=\mathrm{Pr}[\omega^2-br_H-i\omega(b+1)]\ .$$

Thus, if Eq. (45) is satisfied, no secularity appears in Eq. (44), at least through terms of order ε^3. We represent $A(T)$ in polar form: $A(T)=R(T)e^{i\theta(T)}$, where R and θ are real. What is of particular interest here is the behavior of the amplitude R. Substituting into (45) and equating real and imaginary parts, leads finally to a decoupled equation for R alone. Omitting details, this equation may be written in the form

$$\frac{dR}{dT}=\Phi R+\Psi R^3\ , \tag{46}$$

where Φ and Ψ are real quantities given by

$$\Phi=\mathrm{Re}\left\{\frac{br_H[(1+V_H)c_3-W_Hc_2]}{2X_H(c_1+V_Hc_2+W_Hc_3+Q_Hc_4)}\right\}\ ,$$

$$\Psi=\mathrm{Re}\left\{\frac{c_3X_H[(V_H+1)\alpha+\chi+\beta V_H^*]-c_2[W_H(X_H\alpha-2)+\beta-(1+2i\omega)\chi-W_H^*(1-x_H\beta)]}{X_H(c_1+V_Hc_2+W_Hc_3+Q_Hc_4)}\right\}\ ,$$

and whose sign determines whether a limit cycle is bound to be numerically observed or not. Given the complexity of these expressions, an analytical assessment of their value is practically impossible. We hence resort to numerical representation of the Φ and Ψ behavior.

Figures 3(a) and 3(b) display, respectively, the behavior of Φ and Ψ as a function of De for the same values of the Prandtl number as in Fig. 2 (the curves corresponding to $\mathrm{Pr}=35$ are omitted for clarity; their presence do not generate any new insight). Figure 3(a) shows that the quantity Φ remains positive for any value of De and Pr. Its overall value, however, tends to decrease as Pr decreases. Whether this tendency is maintained until Φ becomes negative for smaller Pr value remains to be established. The Ψ curves are shown in Fig. 3(b). All curves indicate a change in sign at some De value. Note that for the range of De values when $\Psi<0$, the limit cycle is stable and a periodic orbit is detected by the numerical solution as we shall see below. For small De value, all curves show that Ψ is positive. This is typically the case of a Newtonian fluid, for which no periodic orbit is detected. The value of De at which there is a change in sign of Ψ appears to decrease as Pr increases. This tendency is maintained for higher Pr values (not shown), and eventually (for roughly $\mathrm{Pr}>50$) Ψ remains negative for *all* values of the Deborah number. This important observation clearly indicates that, even for Newtonian fluids, periodic behavior can emerge but cannot be detected by strictly Newtonian (Lorenz) equations. For $\mathrm{Pr}=4.5$ (and possibly for smaller Pr values), Ψ becomes positive again reflecting an absence of periodic motion.

V. NUMERICAL RESULTS

In the light of the stability picture established on the basis of the analysis presented in the preceding section, we now turn to the numerical solution of Eqs. (22)–(25). Our aim is to elucidate further on the influence of fluid elasticity or normal stress on the conditions for onset of chaotic motion for weakly elastic fluids ($\mathrm{De}<\mathrm{De}^c$). For completeness, we will briefly examine first the flow at a very small Deborah number and $\mathrm{Pr}=10$, which is essentially that obtained from the Lorenz equations. The effect of weak elasticity will then be examined for the same Prandtl number. Given the important qualitative difference initiated by raising the Prandtl number (see Figs. 2 and 3), we will also examine the flow for $\mathrm{Pr}=25$.

A. Close to the Newtonian limit ($\mathrm{Pr}=10$, $\mathrm{De}=0.001$)

In the Newtonian limit, Eqs. (22)–(25) cannot be solved by simply setting De to zero, since this limit leads to a singularity in the equations [25]. For this reason, the value of De is set equal to 0.001. The stability of the solution near the origin (in phase space) may be inferred from Eq. (31), which indicates that for $r<1$, the origin is stable. As r exceeds unity the origin loses its stability, and the solution converges to either C_1 or C_2 depending on

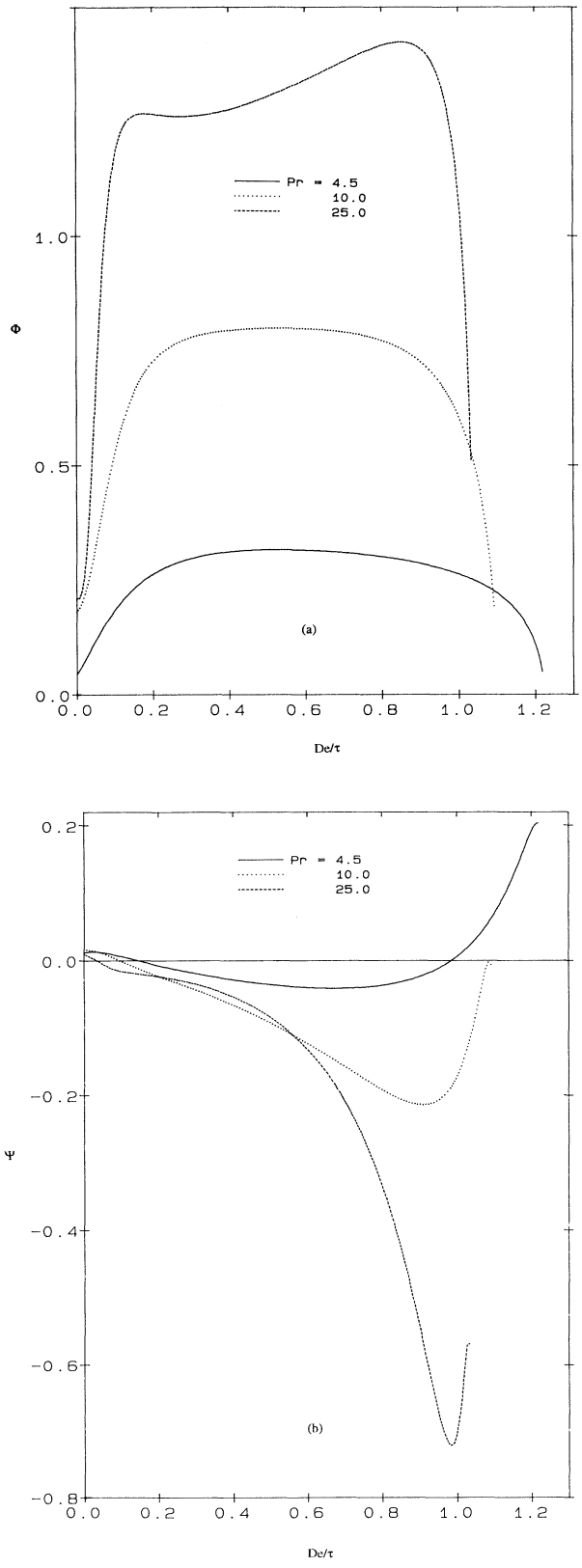

FIG. 3. Stability of the periodic orbit at the birth of the Hopf bifurcation. The limit cycle is stable only if Φ and Ψ are of opposite sign.

the initial conditions. Figure 4(a) shows the behavior for $r=10$, with C_1 being the limit point. As r increases, the solution undergoes a homonclinic bifurcation as shown in Fig. 4(b) for $r=14$. At $r=r_H^{\text{Newt}}\approx 24.74$, a Hopf bifurcation emerges with a loss of stability of all three fixed points. For a substantial range of r values beyond r_H^{Newt} no stable periodic solution is detected numerically. The reason can be seen from Eq. (46) and Figs. 3(a) and 3(b). The figures show that for De=0.001 (Pr=10), both Φ and Ψ are positive. Thus, the nonlinear term in Eq. (46) does not have any stabilizing influence on the limit cycle (leading to a backward bifurcation). Figure 4(c) shows the solution in phase space for $r=28$ as it is confined to the Lorenz attractor. The effect of fluid elasticity is next examined in comparison with the Newtonian picture just summarized.

B. Quasiperiodicity and chaos (Pr=10, De=0.022)

We now examine the flow when the Deborah number exceeds the critical value for the solution to become periodic after the onset of the Hopf bifurcation. We fix Pr=10 in order to compare the present flow with the Newtonian flow above. In this case, Fig. 3 indicates that a periodic orbit is bound to be detected numerically when De>0.01. We thus fix the value at $r_H=3.65$ with initial (dimensionless) angular frequency $\omega=4.747$. The phase portrait and power spectrum for $r=3.9$ are shown in Fig. 5. The trajectory in the phase plane (X,Y) clearly shows a periodic orbit. The fundamental frequency of the limit cycle is shown in Fig. 5(b) of (dimensionless) value equal to 0.68 compared to the value $\omega/2\pi=0.76$ predicted by Eq. (36b). The difference is due to nonlinear effects. These nonlinearities give rise to the distortion in the periodic orbit and the additional harmonics in Fig. 5(b).

When r exceeds a certain critical value, the periodic orbit (around C_1, say) begins to lose its stability. The trajectory is attracted toward a periodic orbit (around C_2) in a manner similar to homoclinic bifurcation. Further increase in r leads to complete instability of the two periodic orbits around C_1 and C_2. Figure 6 illustrates the beginning of loss of periodicity at $r=4.1$ which is accompanied by a thickening of the phase trajectory and weak modulation in the time signal (not shown). The loss of periodicity becomes clearer when r increases further. Figure 7 shows the quasiperiodic solution at $r=4.3$. The phase trajectory tends to fill up a wider bounded region (a two-dimensional torus) in the (X,Y) plane as depicted in Fig. 7(a). Additional amplitude modulation is observed, although weak, as indicated by the power spectrum in Fig. 7(b). There is a second fundamental frequency $f_2<f_1$ with a slight shift in the f_1 value to the right. The spectrum shows peaks at the combination frequencies of $mf_1+nf_2(m,n=0,\pm1,\pm2,\ldots)$. At $r=4.4$, a third fundamental frequency f_3 emerges in the power spectrum in Fig. 8(b) accompanied by a broadening around f_1 and f_2, thus indicating the onset of weak chaotic behavior as can be confirmed from the broadening of the phase trajectory in Fig. 8(a). When r is in-

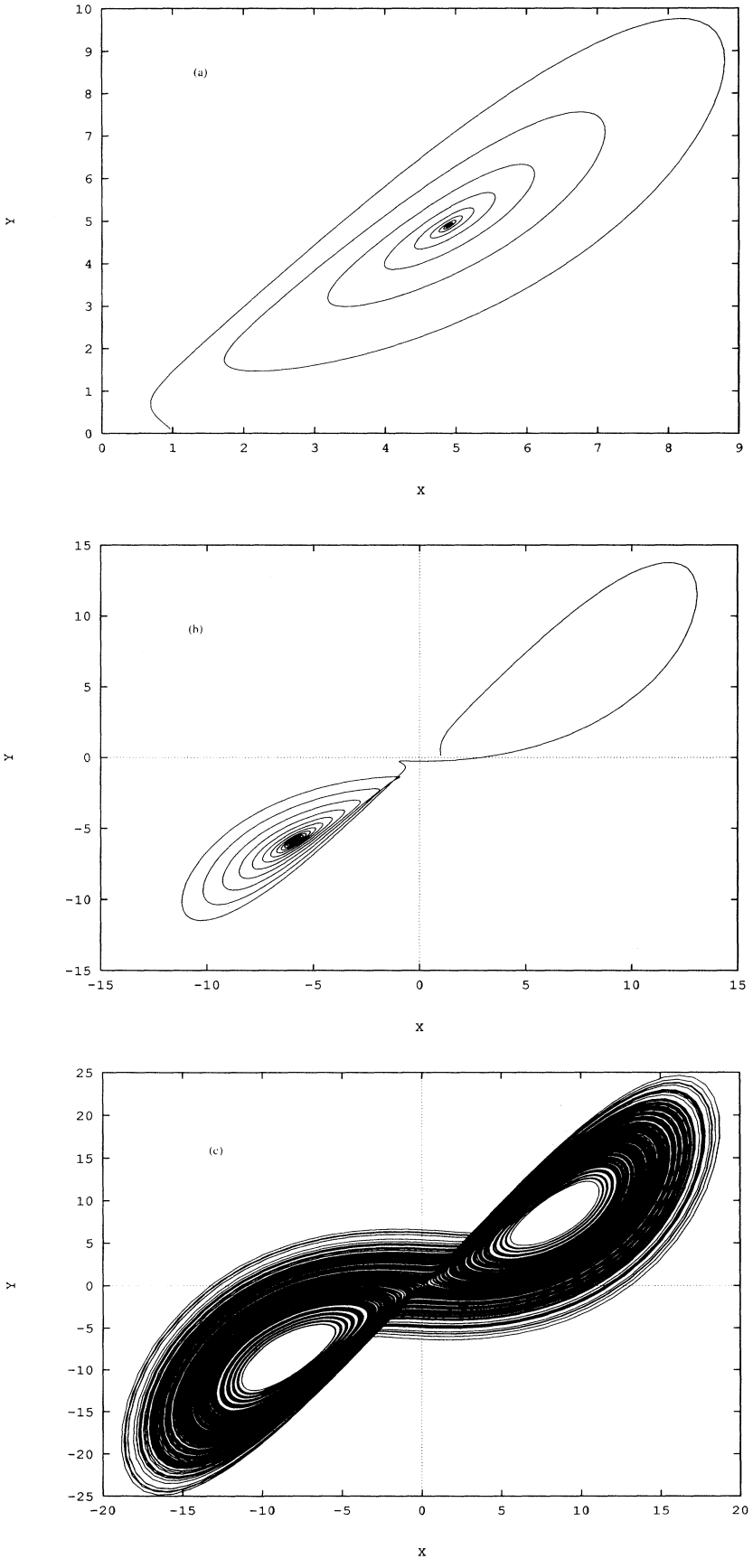

FIG. 4. Solution behavior close to the Newtonian limit (De=0.001) and Pr=10. Phase trajectory in the (X, Y) plane for $r=10$, leading to stable convection (a); $r=14$, showing a homoclinic bifurcation (b); and $r=28$, displaying chaotic behavior (c). This sequence is essentially the same as the one based on the Lorenz equations.

creased to 4.6, chaotic behavior becomes particularly obvious from the phase portrait in Fig. 9(a). The power spectrum in Fig. 9(b) shows a significant decrease in amplitude and additional broadening at the fundamental frequency f_1. The third fundamental frequency f_3 disappears together with the higher harmonics.

C. Period doubling and chaos (Pr=25, De=0.003)

We have observed earlier (see Fig. 3) that the critical value of De, for periodic behavior to set in, becomes increasingly smaller as the Prandtl increases. Thus, even supposedly "Newtonian" flows appear bound to exhibit periodicity in the higher Pr range. While such periodic behavior is not predicted by the Lorenz equations, the presence of a relatively small level of fluid elasticity can account for it. To illustrate this fact, we examine the flow at Pr=25 and fix the Deborah number to a small value De=0.003. In this case, the transition to chaos occurs through a succession of period doubling.

The sequence of period doubling is shown in Figs. 10 to 13 for the range $r \in [45,53]$ of the Rayleigh number. Note that in this case, a Hopf bifurcation emerges at $r = r_H = 38$ (see Fig. 2), with initial frequency

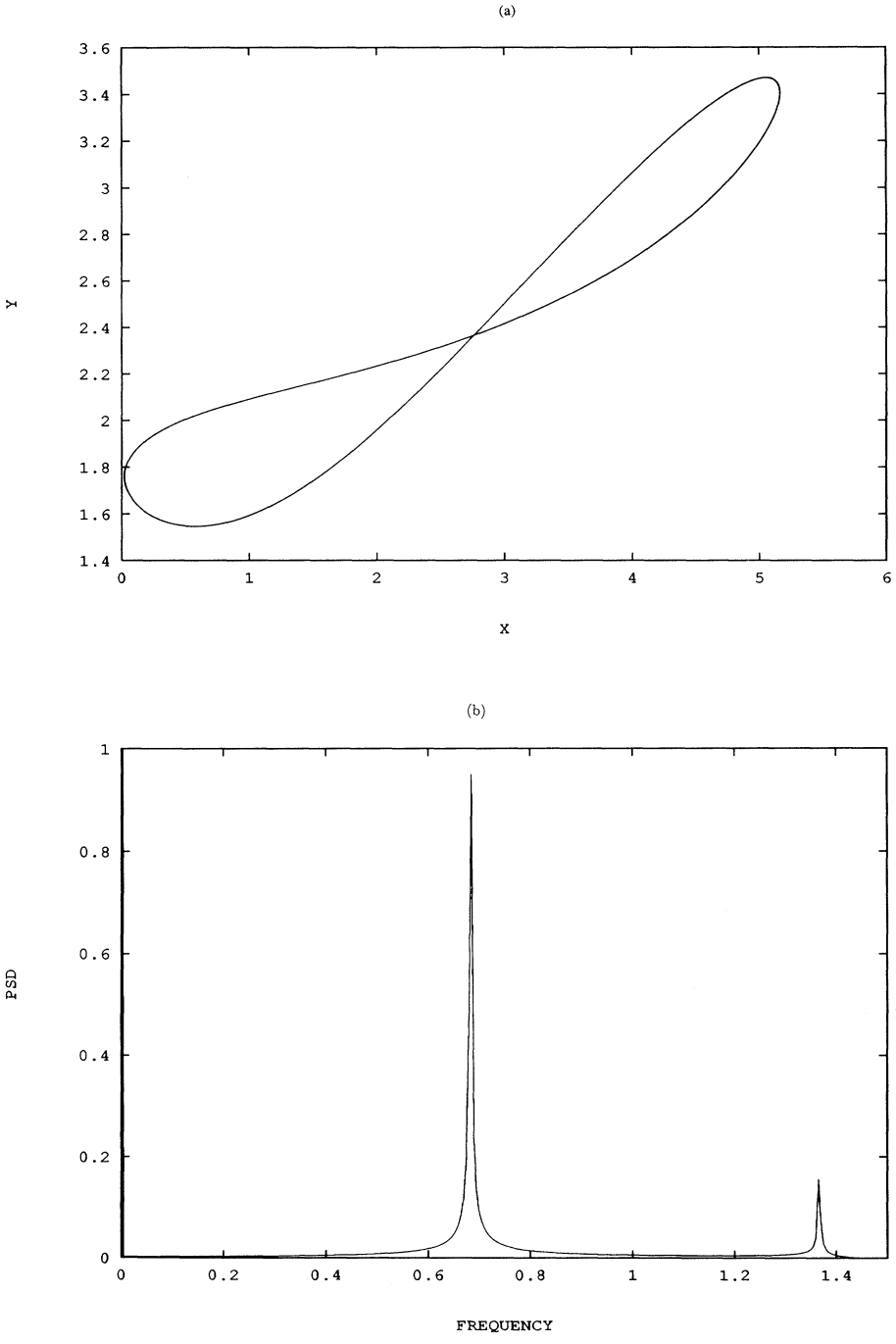

FIG. 5. Periodic solution for De=0.022, Pr=10, and $r=3.9$. Phase trajectory on a single loop in the (X, Y) plane showing some distortion (a); and the presence of one harmonic in the power spectrum density (b).

$f=\omega/2\pi=2.48$. Figure 10 shows a period-1 solution at $r=45$. The phase trajectory in the (X,P) plane is locked onto a single closed orbit. The slight distortion in the orbit and the presence of higher harmonics in the power spectrum in Fig. 10(b) indicate the presence of weak nonlinearities. The value of the fundamental frequency f in the power spectrum is 2.25, which is slightly smaller than the one predicted by linear analysis. As r is increased, the period-1 motion bifurcates into a period-2 motion and appears as shown in Fig. 11 for $r=50$. The trajectory in Fig. 11(a) exhibits two loops, and the power spectrum in Fig. 11(b) shows peaks at $f/2$ and its multiples. The period-4 motion at $r=52$ is shown in Fig. 12. As the Rayleigh number is further increased to $r=53$, the period doubling reaches the accumulation point, and gives way to a chaotic solution as can be seen from Fig. 13. In this case, the trajectory in phase space [Fig. 12(a)] does not form a closed orbit. It does suggest, however, that the solution has undergone a large number of period doubling. The power spectrum shows the $\frac{1}{8}$ subharmonics and its multiples surrounded by continuous spectral segments. This confirms that the period-doubling bifurca-

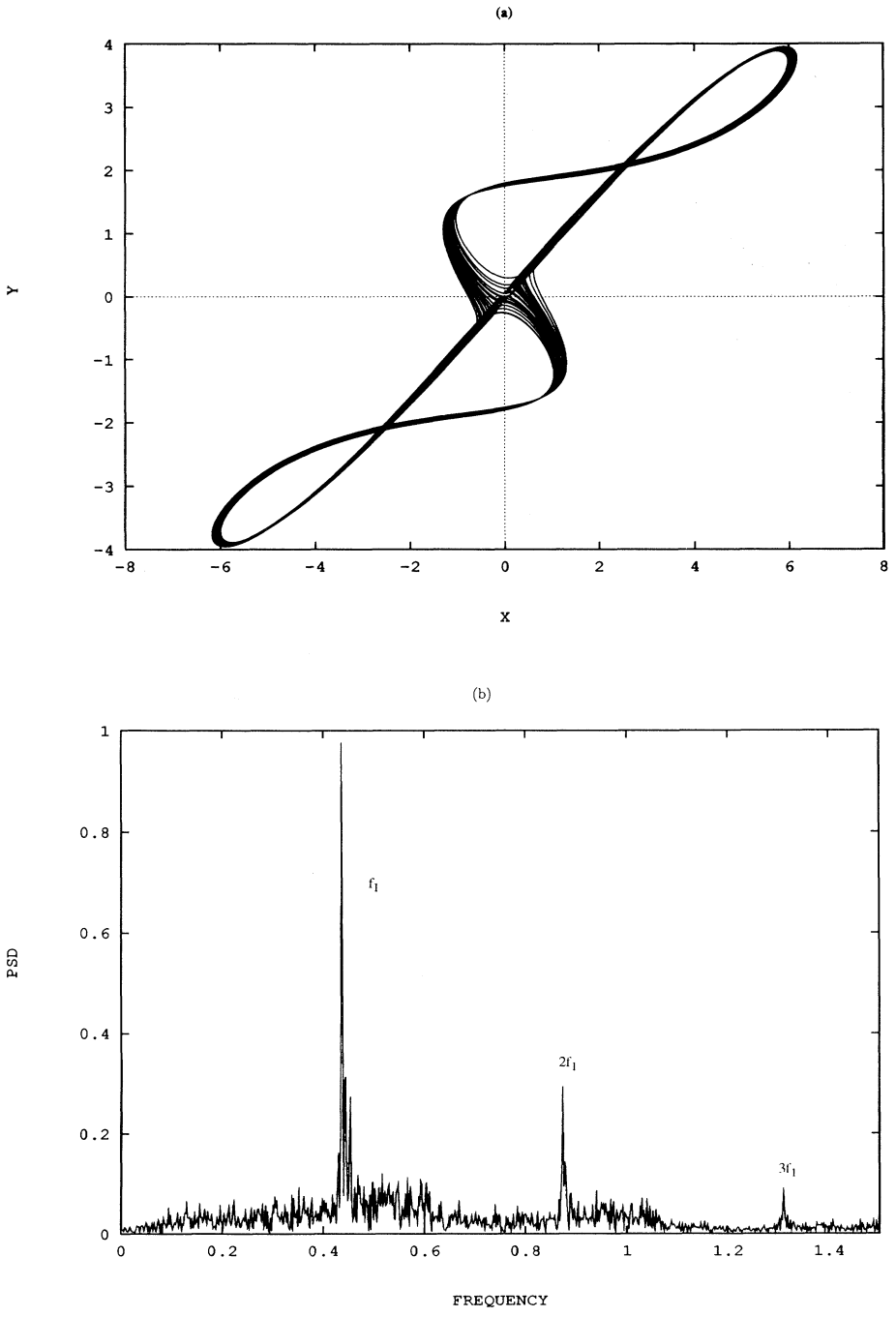

FIG. 6. Loss of stability of the limit cycle for De=0.022, Pr=10, and $r=4.1$. Phase trajectory showing an almost periodic orbit (a); with two harmonics in the power spectrum (b).

tion is responsible for the gradual spreading of the spectrum and the broadening of the trajectory in phase space. The continuous spectral segments around subharmonic components imply a transition to chaos in conjunction with the period-doubling bifurcation. This succession of period doubling, and the onset of chaos at an accumulation value of a driving parameter, is known as the Feigenbaum route [26], and has been observed in many experiments [27].

VI. DISCUSSION AND CONCLUSION

Fluid elasticity constitutes a fundamental characteristic of any fluid and not just polymeric liquids. Some of the more recent experimental estimates of fluid elasticity indicate that some of the supposedly "Newtonian" fluids possess a level of elasticity several orders of magnitude higher than has previously been believed [9–12]. Molecular [7,28,19] and phenomenological [20] theories suggest

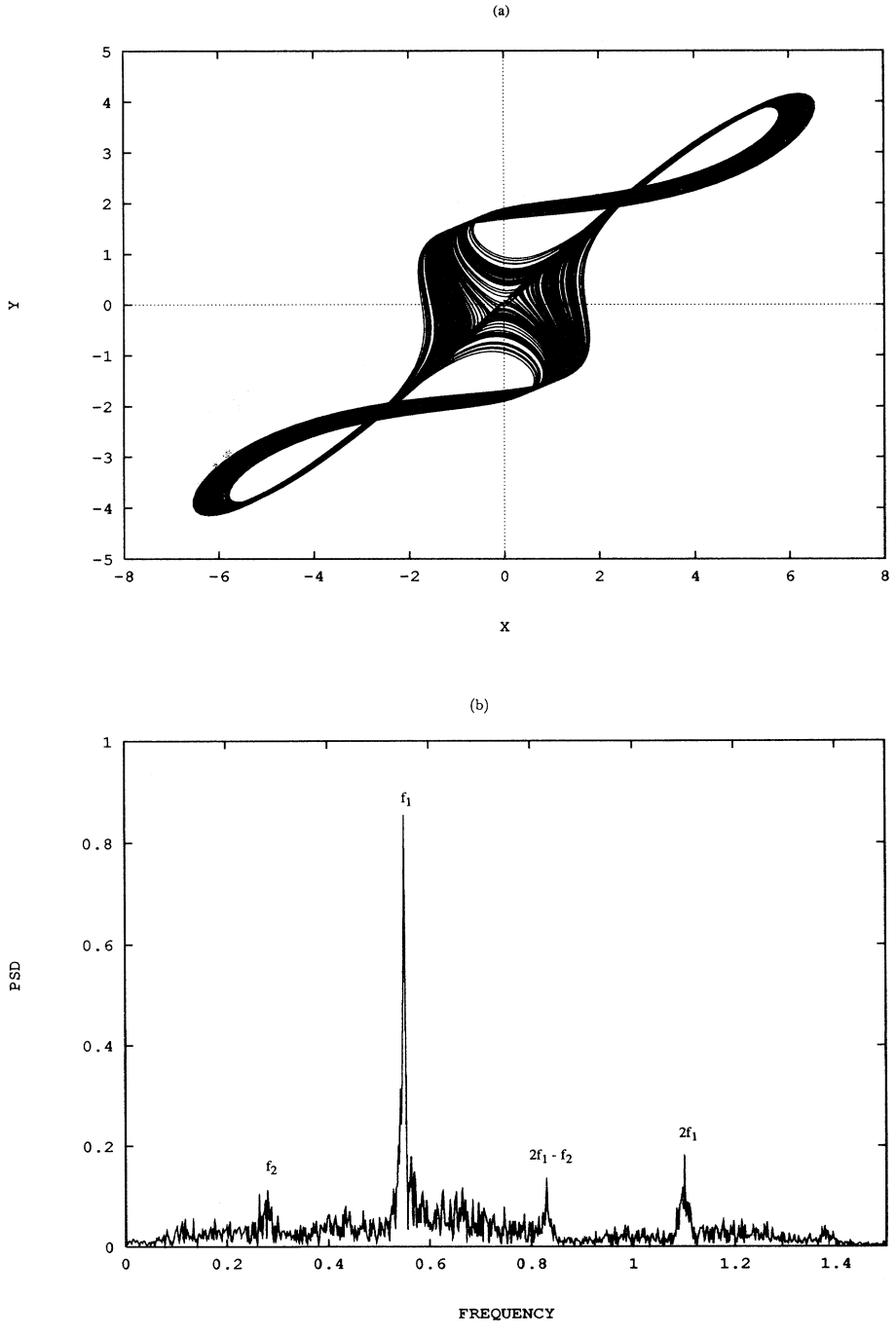

FIG. 7. Quasiperiodicity for De=0.022, Pr=10, and $r=4.3$. A wider region is filled up by the phase trajectory (a). Fourier spectrum (b) showing two fundamental frequencies $f_1=0.5501$ and $f_2=0.2803$ and harmonics.

that the normal stress coefficient (which is a measure of elasticity) representing normal stress effects may be strongly dependent on thermodynamic gradients. In particular, normal stresses tend to increase with shear rate. Thus, one should expect that the effect of fluid elasticity or normal stresses becomes more significant in the transition and turbulent regimes. In this case, the Navier-Stokes equations may not constitute a realistic model to examine chaotic or turbulent flow. If we believe the inadequacy of the Navier-Stokes equations in the presence of large gradients, we immediately face the question regarding the choice of a suitable constitutive model for describing turbulent flow.

Kinetic theory has been a major theoretical tool in the development of constitutive models. Hydrodynamic equations such as the Navier-Stokes equations are accorded a kinetic theory foundation by the Boltzmann equation and the Chapman-Enskog solution [28]. Grad's moment method leads to a Maxwell type constitutive equation [5]. It is well established that the first-order

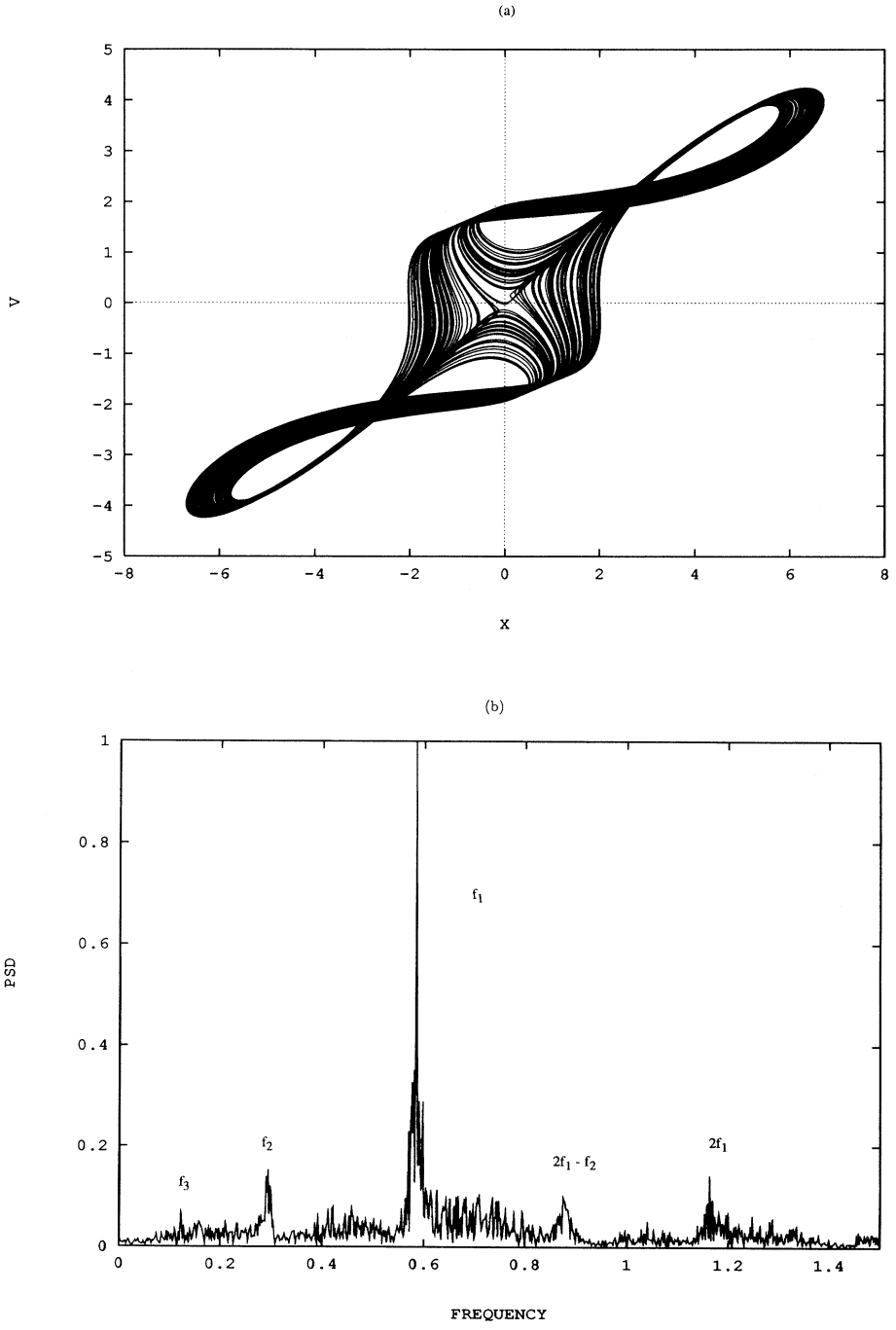

FIG. 8. Quasiperiodicity and weak chaos for De=0.022, Pr=10, and $r=4.4$ as confirmed from the phase trajectory (a). The Fourier spectrum (b) shows three fundamental frequencies of $f_1=0.5842$, $f_2=0.2938$, and $f_3=0.1226$, and peaks at their combinations.

Chapman-Enskog solution leads to constant transport coefficients, particularly the viscosity, which makes the Navier-Stokes equations applicable for flows close to equilibrium. This argument, of course, is not applicable when a shear rate dependent viscosity is simply imposed in the momentum equation. Indeed, for flows far from equilibrium, one is forced to adjust the Navier-Stokes equations by introducing an effective viscosity, explicitly through a shear rate dependent viscosity, or implicitly through a viscoelastic equation for stress. This has been the route taken for most of the constitutive models to describe turbulent flows. More generally, in the macroscopic description of irreversible processes, one aims at obtaining a theory completely consistent with the thermodynamic laws, more particularly the second law, since no irreversible process is possible if it violates the thermodynamic laws. In the modified moment method of solution for the (generalized) Boltzmann equation for (dense) dilute fluids [7,8], approximate solutions to the kinetic equation are obtained in such a way that the H theorem is satisfied by them. The modified moment method yields a constitutive equation for stress that generalizes

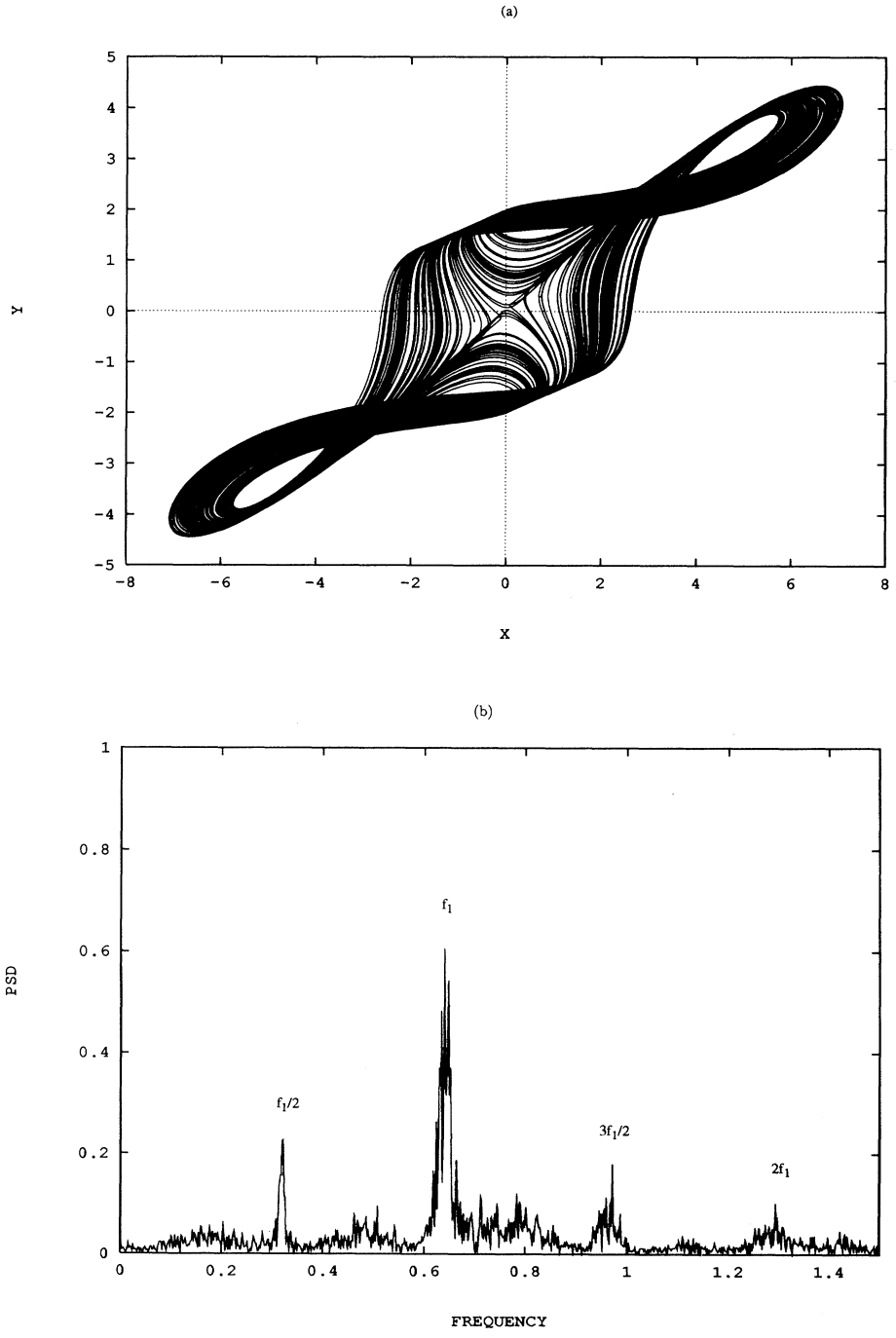

FIG. 9. Chaotic motion for De=0.022, Pr=10, and $r=4.6$ as confirmed from the phase trajectory (a). The Fourier spectrum (b) shows additional broadening at f_1 and frequency locking.

Newton's law of viscosity and Maxwell's equation. This equation consists of the usual terms collectively called the convective terms, and a dissipative term which originates from the collision term in the (generalized) Boltzmann equation. The nonlinear collision integral is approximated using a cumulant expansion method. To first order in the cumulant approximation, the collision integral yields dissipative terms in the stress equation which are proportional to a hyperbolic sine function whose argument is simply the Rayleigh-Onsager dissipation function [1]. Therefore, the cumulant expansion yields a dissipative term that amounts to a partial resummation of infinite Chapman-Enskog series for the collision term in the (generalized) Boltzmann equation. The resulting transport coefficients (of viscosity and normal stress) are highly nonlinear and strongly dependent on shear rate. One can, however, show that for the weakly nonlinear flow (weak dependence of transport coefficients on shear rate), the generalized hydrodynamic equation for stress reduces to the (upper-convected) Maxwell equation. It is precise-

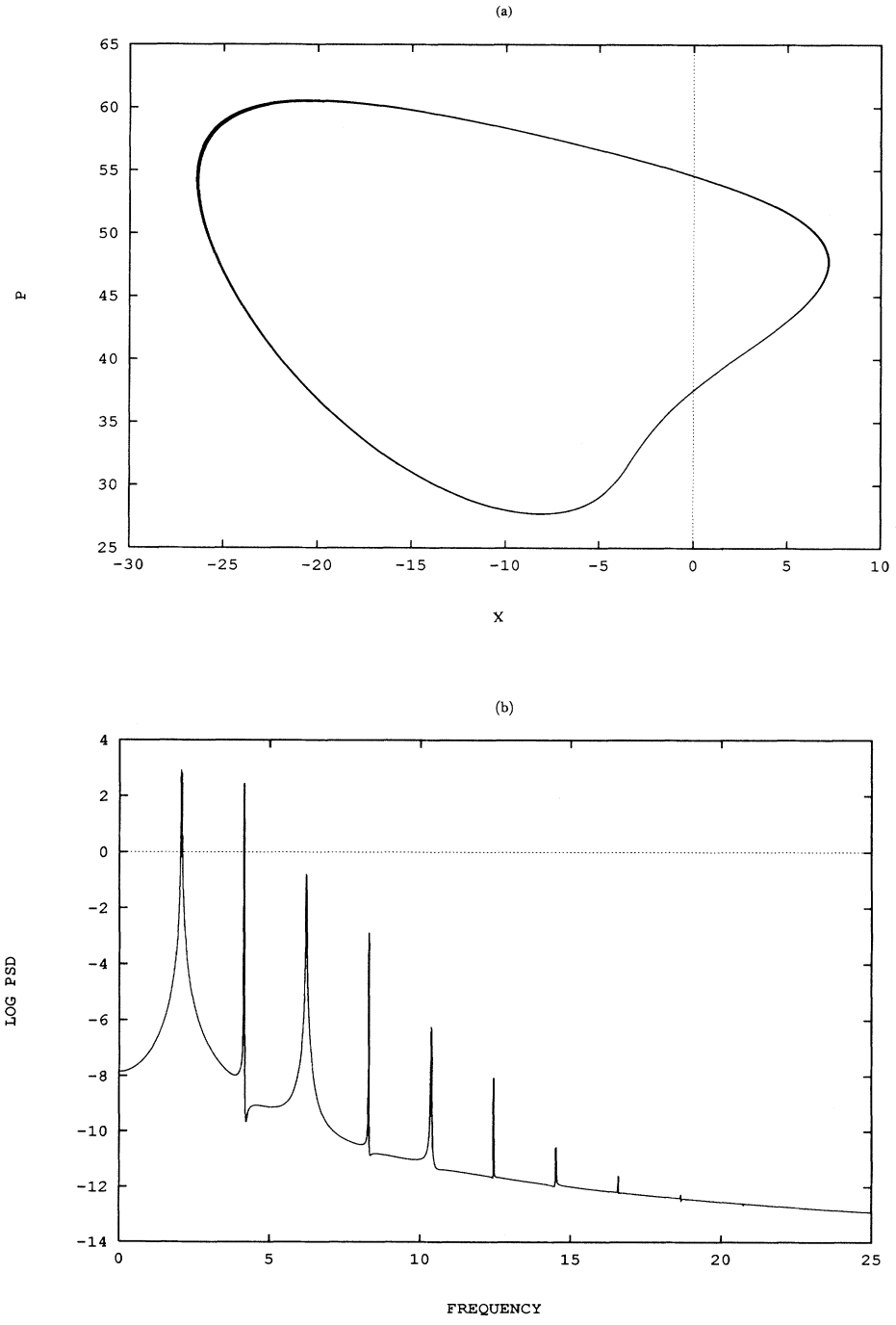

FIG. 10. Period-1 motion for De=0.003, Pr=25, and $r=45$. Phase trajectory in the (X,P) plane (a); and corresponding Fourier spectrum (b) showing fundamental frequency f and harmonics.

ly for this reason that we have limited the present investigation to the weakly nonlinear transition flow of a Maxwellian fluid.

The use of the UCM equation to examine the onset of chaotic motion will set the foundation and tone for a more thorough investigation using the more realistic constitutive models. Such models, whether molecular based or phenomenological, must account for the nonlinear dependence of viscosity and normal stress coefficients on shear rate as argued above. Despite its limited validity, the UCM equation gives rise to important qualitative flow phenomena not predicted by the Navier-Stokes equations. The emergence of quasiperiodicity and period doubling are just manifestations of how altered the road to chaotic motion can be when viscoelastic effects are accounted for. More importantly, such scenarios are experimentally observed and cannot be recovered through the Navier-Stokes equations. Furthermore, based on the numerical results in the present study, even the presence of minute elastic effects in the constitutive equation appears

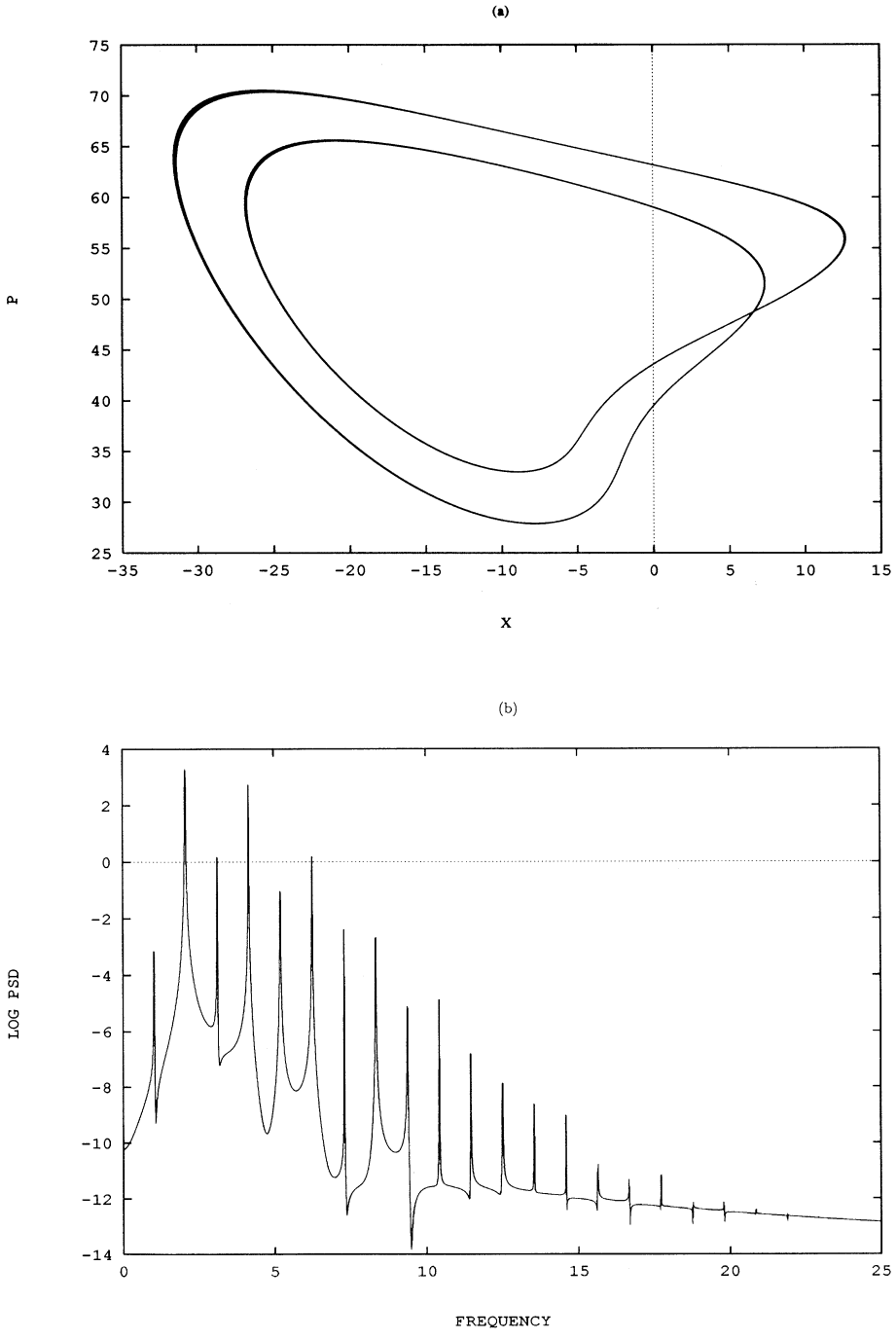

FIG. 11. Periodic-2 motion for De=0.003, Pr=25, and $r=50$. Phase trajectory in the (X,P) plane (a); and corresponding Fourier spectrum (b) showing fundamental frequencies f, $f/2$, and harmonics.

to lead, at least qualitatively, to a more accurate theoretical prediction. Such a closer agreement between theory and experiment should be expected when viscoelastic effects are accounted for, as we next argue, even when only supposedly "Newtonian" fluids are involved.

First, we observe that a viscoelastic equation for stress does change the type of the system of equations describing the whole flow field. The change from parabolic to hyperbolic type when the Maxwell equation is used [29] is of far reaching consequence on the flow, particularly during transition. Experimental evidence strongly suggests the presence of a characteristic behavior common to the better understood routes to chaotic motion, namely, periodic behavior. It is sufficient to just examine the three most common scenarios involving intermittent behavior, quasiperiodicity, and period doubling, to see that chaotic motion usually sets in after the flow has undergone periodic behavior. This seems to indicate that the flow in the transition regime exhibits periodic motion that cannot be recovered by the (parabolic or diffusive) Navier-Stokes equations suggested. Therefore, the discrepancy between the solution to the Lorenz equations

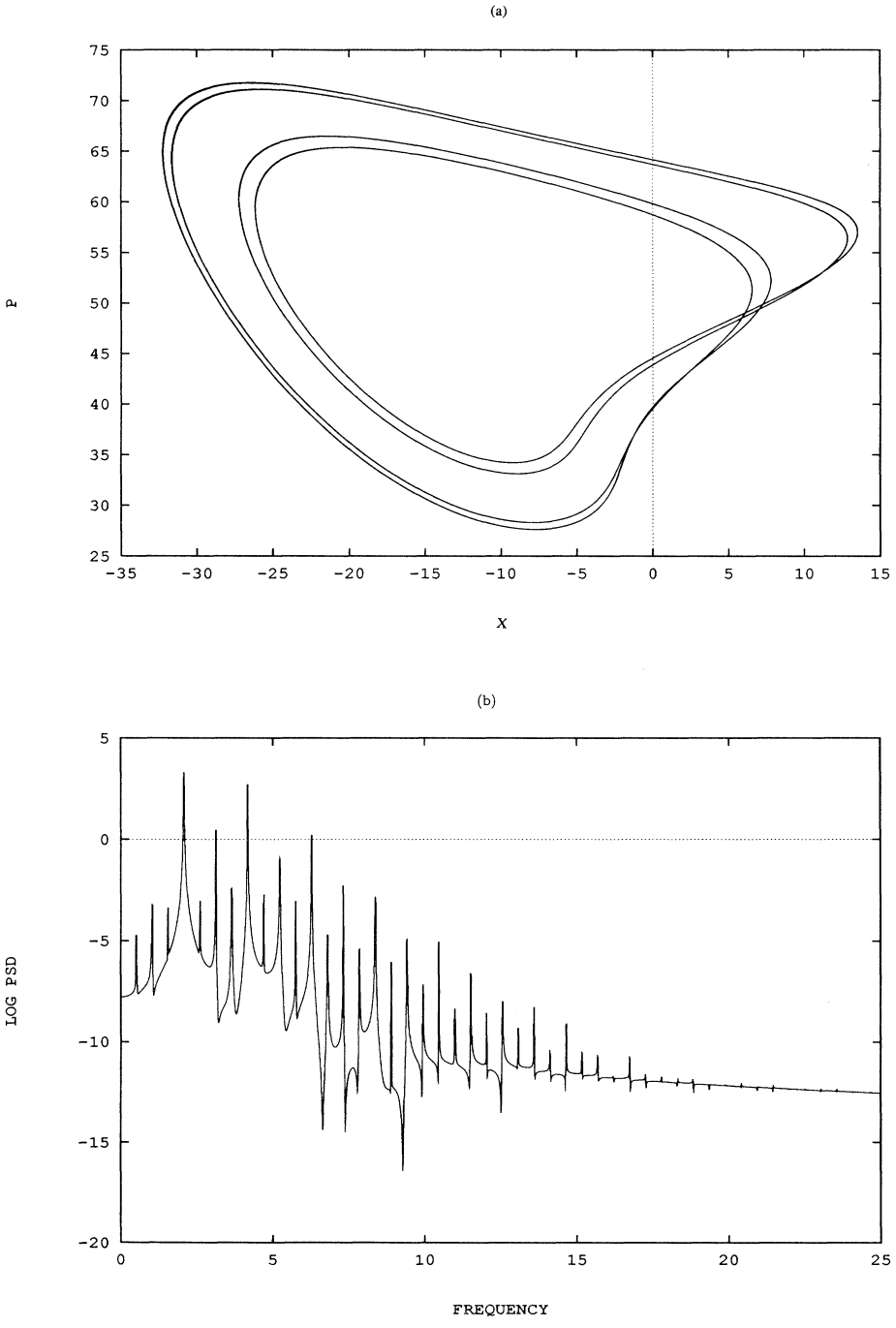

FIG. 12. Period-4 motion for De=0.003, Pr=25, and $r=50$. Phase trajectory in the (X,P) plane (a); and corresponding Fourier spectrum (b) showing fundamental frequencies f, $f/2$, $f/4$, and harmonics.

(27) and experiment is most likely not due exclusively to the level of truncation in the (Fourier) representation of the solution, but to the very diffusive character of the Navier-Stokes equations at the outset. Second, even for low molecular weight fluids which possess a relatively small relaxation time, one cannot ignore viscoelastic effects and simply set De=0 in the viscoelastic equations to recover the Lorenz solution from Eqs. (22)–(25), because the latter equations are singular in the limit De→0. A similar argument holds for the Maxwell and Navier-Stokes equations. This seemingly purely mathematical fact is of great physical consequence. Indeed, additional calculations based on Eqs. (22)–(25) show that similar spatiotemporal structures and stability pictures to the ones reported in Sec. V are obtained when the Deborah number is set very small but not zero, except that in this case, the corresponding critical values of the Rayleigh number or the Prandtl number for onset of periodic motion must be higher the smaller De is (see Fig. 2). Third, we come to an interesting point. The severity of truncation in the Fourier representation (17)–(21) has made it such that the nonlinear convective terms in Eq.

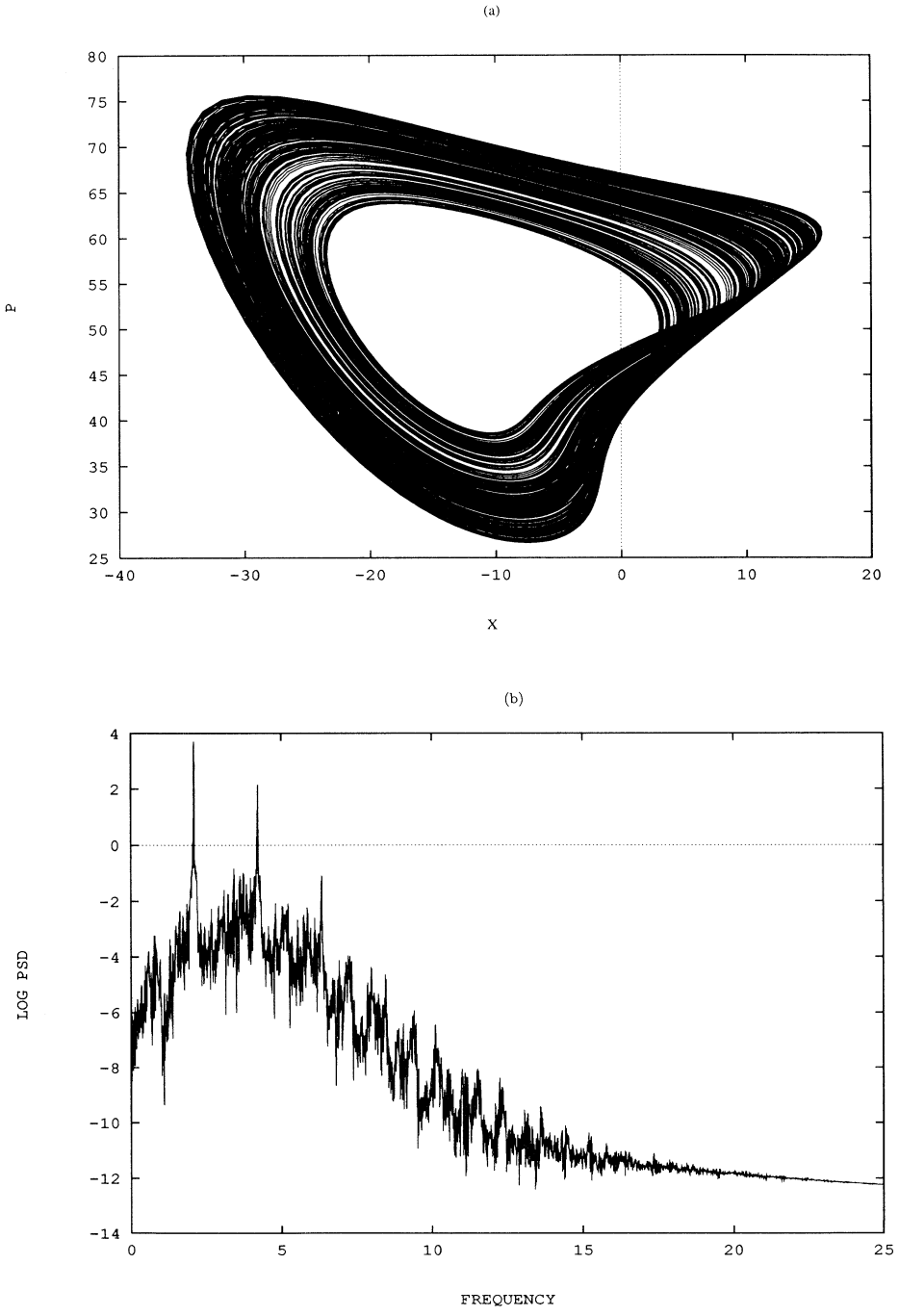

FIG. 13. Chaotic motion for De=0.003, Pr=25, and $r=50$. Phase trajectory in the (X,P) plane (a); and corresponding Fourier spectrum (b) showing still the fundamental frequency f and harmonics, with significant base broadening.

(5) did not survive in the final Eqs. (22)–(25). Thus, the nonlinearities in the viscoelastic equations stem from the convective terms in the energy equation, and are the same as those in the Lorenz equations (27). We may as well have started then with a linear Maxwell equation for stress, and the results would not have changed. What is interesting to observe is the fact that the major distinction between the Lorenz and viscoelastic flows is of nonlinear nature: quasiperiodicity and period doubling. This is a rather intriguing fact, that new nonlinear phenomena have been brought into existence by the presence of an additional *linear* equation, namely, Eq. (25). Whether the presence of nonlinear terms in a more realistic constitutive equation will play a dominantly significant role on the spatiotemporal behavior remains an open issue. For one, the steady-state solution(s) will be altered because of additional nonlinearities.

In conclusion, we have examined in the present study the influence of fluid elasticity or normal stress on the destabilization of steady convection and onset of chaotic behavior for weakly elastic flows. The four-dimensional truncated model embedding Maxwell equation for stress constitutes a generalization of the Lorenz model for Newtonian fluids. It is found that for a small but nonvanishing Deborah number De, a Hopf bifurcation sets in at a Rayleigh number which generally tends to decrease with De. Thus, elasticity appears to have a destabilizing effect (see also Ref. [30]). This is not always the case, however, in the moderately high Prandtl range. A multiple-scales perturbation analysis is carried out around the onset of the Hopf bifurcation to determine the stability of the resulting periodic orbit. The limit cycle was found to be generally stable except when the Deborah number is very small (also in the limit of the Lorenz equations). It is clear, however, form the numerical values of De that practically all fluids are predicted to display periodic behavior, a fact not reflected when elasticity is entirely neglected. The value of the Prandtl number was found to be a determining factor in the manner transition to chaotic behavior occurs. Chaotic motion was shown to set in via quasiperiodicity and periodic doubling.

Whether low molecular weight of supposedly Newtonian fluids in practice exhibit viscoelastic effects in the transition regime can only be confirmed through direct comparison with experiment. The present formulation and numerical calculations can only bring out qualitatively some of the fundamental and nonlinear character inherent to any fluid subject to high shear flow. In this respect, the present results seem to indicate that some of the routes to chaos observed in the thermal convection of "Newtonian" fluids, in particular the quasiperiodicity and period-doubling scenarios, can be recovered if elastic or normal stress effects are accounted for. A more thorough and realistic formulation must account for lateral boundaries, incorporate stick and not slip conditions at the walls, include many more modes in the Fourier representation of solution, and use a more accurate constitutive model including shear thinning.

[1] R. P. de Groot and P. Mazur, *Non-equilibrium Thermodynamics* (Dover, New York, 1984).

[2] K. Nanbu, Phys. Fluids A **27**, 2632 (1984).

[3] S. Stefanov and C. Cercignani, J. Fluid Mech. **256**, 199 (1994).

[4] A. Vedavarz, S. Kumar, and M. K. Moallemi, J. Heat Transfer **116**, 221 (1994).

[5] H. Grad, Comm. Pure Appl. Math. **2**, 331 (1949).

[6] J. R. Dorfman and H. van Beijren, in *Statistical Mechanics,* edited by B. J. Berne (Plenum, New York, 1977), Part B, pp. 65–175.

[7] B. C. Eu, *Kinetic Theory and Irreversible Thermodynamics* (Wiley, New York, 1992).

[8] B. C. Eu and R. E. Khayat, Rheol. Acta **30**, 204 (1991).

[9] B. V. Derjaguin, U. B. Bazaron, Kh. D. Lamazhapova, and B. D. Tsidypov, Phys. Rev. A **42**, 2255 (1990).

[10] D. D. Joseph, A. Narain, and O. Riccius, J. Fluid Mech. **171**, 289 (1986).

[11] D. D. Joseph, O. Riccius, and M. Arney, J. Fluid Mech. **171**, 309 (1986).

[12] D. D. Joseph, O. Riccius, and M. Arney, Rheol. Acta **26**, 96 (1987).

[13] (a) R. E. Khayat and B. C. Eu, Phys. Rev. A **38**, 2492 (1988); (b) **39**, 728 (1989); (c) **40**, 946 (1989).

[14] R. E. Khayat, in *Developments in Non-Newtonian Flows,* edited by D. Siginer, W. E. Van Arsdale, M. C. Altan, and A. N. Alexandrou (American Society of Mechanical Engineers, New York, 1993), AMD-Vol. 175, pp. 71–83.

[15] E. N. Lorenz, J. Atmos. Sci. **20**, 130 (1963).

[16] R. E. Khayat, J. Non-Newt. Fluid Mech. **53**, 227 (1994).

[17] J. Carr, *Applications of Center Manifold Theory* (Springer-Verlag, New York, 1981).

[18] C. Sparrow, *The Lorenz Equations* (Springer-Verlag, New York, 1983).

[19] R. B. Bird, R. C. Arsmtrong, and C. F. Curtis, *Dynamics of Polymeric Liquids: Volume 2 Kinetic Theory* (Wiley, New York, 1987).

[20] R. B. Bird, R. C. Armstrong, and O. Hassager, *Dynamics of Polymeric Liquids: Volume 1 Fluid Mechanics* (Wiley, New York, 1987).

[21] H. N. Shirer and R. Wells, *Mathematical Structure of the Singularities at the Transitions Between Steady States in Hydrodynamic Systems* (Springer-Verlag, Heidelberg, 1980).

[22] S. F. Liang and A. Acrivos, Rheol. Acta **9**, 447 (1970).

[23] R. E. Khayat (unpublished).

[24] A. C. Newell and J. A. Whitehead, J. Fluid Mech. **38**, 279 (1969).

[25] R. E. Khayat, Quart. J. Mech. Appl. Math. **47** (3), 341 (1994).

[26] M. J. Feigenbaum, Commun. Math. Phys. **77**, 65 (1980).

[27] H. G. Schuster, *Deterministic Chaos* (Verlagsgesellschaft, Weinheim, 1987).

[28] S. Chapman and T. G. Cowling, *Mathematical Theory of Non-Uniform Gases,* 3rd ed. (Cambridge University Press, London, 1970).

[29] D. D. Joseph, in *Amorphous Polymers and Non-Newtonian Fluids,* edited by C. Dafermos, J. L. Ericksen, and D. Kinderlehrer (Springer-Verlag, New York, 1987).

[30] R. G. Larson, Rheol. Acta **31**, 213 (1992).